

The Unusually Stable B_{100} Fullerene, Structural Transitions in Boron Nanostructures, and a Comparative Study of α - and γ -Boron and Sheets

C. Özdogan,[†] S. Mukhopadhyay,[‡] W. Hayami,[§] Z. B. Güvenç,^{||} R. Pandey,[‡] and I. Boustani*,^{†,⊥}

Department of Computer Engineering, Çankaya University, Balgat 06530 Ankara, Turkey, Department of Physics, Michigan Technological University, Houghton, Michigan, 49931, National Institute for Materials Science (NIMS), 1-1 Namiki, Tsukuba, Ibaraki 305-0044, Japan, Department of Electronic and Communication Engineering, Çankaya University, Balgat 06530 Ankara, Turkey, and FB C - Mathematik und Naturwissenschaften, Bergische Universität Wuppertal, Gaußstraße 20, D-42097 Wuppertal, Germany

Received: December 8, 2009; Revised Manuscript Received: January 23, 2010

Solid α - B_{12} rhombohedral and γ - B_{28} orthorhombic boron as well as boron nanostructures in the form of spheres, sheets, and multirings beside a ring consisting of icosahedral B_{12} units were investigated using *ab initio* quantum chemical and density functional methods. The structure of the B_{100} fullerene exhibits unusual stability among all noninteracting free-standing clusters, and is more stable than the B_{120} cluster fragment of the γ - B_{28} solid, recently predicted and observed by Oganov et al. (*Nature* 2009, 457, 863). In addition, we compared the stability of the multirings and reported the structural transition from double-ring to triple-ring systems. This structural transition occurs between B_{52} and B_{54} clusters. We confirm that the noninteracting free-standing triangular buckled-sheet is more stable than the γ -sheet, assembled in this work, and than the α -sheet, proposed by Tang and Ismail-Beigi (*Phys. Rev. Lett.* 2007, 99, 115501). In contrast, however, when these sheets are considered as infinite periodic systems, then the α -sheet remains the most stable one.

I. Introduction

The varieties of pure boron in the form of novel solids^{1,2} and of nanostructures as quasiplanar clusters,³ nanosheets,^{4,5} nanotubes,^{6,7} nanoropes,¹² nanospheres,^{8,10,11} nanowires,^{13,14} nanobelts,¹⁵ nanoribbons,^{16,17} nanochains, and quasi-crystals^{18,19} are nowadays some of the best alternatives to carbon fullerenes (CFs) and nanotubes (CNTs) which exhibit superior properties or at least similar versatility as CFs and CNTs. Toward that, boron, being the nearest neighbor to carbon in the periodic table, is nonreactive at room temperature, known with its short covalent radius, multicenter and directed covalent bonds, holds a unique property because of its electron deficient character and thermic properties. Despite the recent discovery of novel solid boron or prediction of novel nanostructures, many forms are still remaining undiscovered. The theoretical methods based on a variety of concepts, ranging from the most accurate *ab initio* methods suited for small or medium sized systems up to semiempirical ones for larger systems enable us to detect, analyze, and optimize most of the materials as inexpensive, fast, and reliable alternatives to experimental methods in materials science. These methods provide an opportunity for “materials engineering”, a systematic understanding and development of new nanoscale materials with desired properties.

The physics and chemistry of boron resembles in its ability to configure and form molecular networks. Unlike carbon, pure bulk boron does not exist in nature and all common boron allotropes were obtained in the laboratory. The most known family of the conventional boron solids is composed of the α -

and β -rhombohedral/tetragonal boron. The α -rhombohedral boron²⁰ is built up from different arrangements of B_{12} icosahedral units and transforms by 1200 °C into the more stable solid β -rhombohedral boron.^{21,22} β -boron is composed of much complicated $B_{12}(B_6)_{12}$ polyhedra.^{23,24} The structure of β -rhombohedral boron consists of B_{12} icosahedra and B_{28} subunits which can be regarded as triplex icosahedra.²⁵ There are several interstitial sites that are partially occupied by single boron atoms; this increases the degree of freedom and, consequently, the entropy. The complexity of the latter structures is due to the fact that the 5-fold rotational symmetry of the icosahedral unit B_{12} is incompatible with lattice periodicity.²⁶ This thermodynamically more stable β -rhombohedral polymorph has a high melting point of around 2450 °C. Both α - and β -rhombohedral boron are semiconductors with measured band gaps of 2 and 1.6 eV, respectively. Further forms of solid boron are the α - and β -tetragonal boron,^{27,28} which are composed of tetrahedral arrangements of B_{12} icosahedra.

The family of the conventional boron solids, mentioned above, becomes a new member. Oganov et al.¹ synthesized a new boron phase called γ - B_{28} under high-pressure and high-temperature conditions for the first time. This new boron solid was later also synthesized by Zarechnaya et al.² under similar conditions. Oganov et al.¹ and Zarechnaya et al.² found that this novel boron crystal is consisting of icosahedral B_{12} clusters and B_2 pairs in an orthorhombic NaCl-type arrangement with the space group *Pnnm* and 28 atoms in the unit cell. They also found that this new phase is stable above 9 GPa and up to 89 GPa, it keeps its structure at room temperature and pressure, and can be quenched to ambient conditions. This new phase of boron should also be more stable than any other boron solids. However, the synthesis of a crystalline phase at high pressure was reported in 1965 by Wentorf²⁹ without performing structure solution or chemical analysis. Nevertheless, he determined the density of this new boron phase to be about 2.52 g/cm³, which

* Corresponding author. E-mail: boustani@uni-wuppertal.de.

† Department of Computer Engineering, Çankaya University.

‡ Michigan Technological University.

§ National Institute for Materials Science (NIMS).

|| Department of Electronic and Communication Engineering, Çankaya University.

⊥ Bergische Universität Wuppertal.

is confirmed by Zarechnaya et al.³⁰ Oganov et al.¹ reported that a phase transformation from α -B₁₂ into γ -B₂₈ occurs at 19 GPa and from γ -B₂₈ into α -Ga type at 89 GPa.

Noncrystalline boron structures at the nanoscale were achieved forming building blocks, systematically constructed from small units, using the so-called bottom-up approach. Systematic *ab initio* investigations on boron systems starting with two atoms and up to a cluster size of a few hundred led to the understanding of the nature of chemical bonds and the mechanism of cluster formation. Hereafter, Boustani predicted, for the first time, the planarity of small boron clusters³¹ and together with Quandt the existence of boron nanotubes,³² hitherto unknown in nature. Boustani showed⁴ that the planarity of these clusters, e.g., the B₁₃ cluster, refers to the stabilizing effect of the π -orbitals of the leading electronic configuration having an aromatic form with electron clouds on both sides of the cluster plan, analogous to benzene. Then, he described a general cluster formation via the so-called “Aufbau principle” (AP)³ which shows how to build up highly stable clusters, sheets, spheres, and nanotubes using small boron clusters as building blocks of nanostructures. In all of these nonicosahedral structures, the boron atoms undergo sp² hybridization which substantiates the planarity and aromaticity of most surfaces of these nanostructures. Incidentally, it is worth mentioning that the “Aufbau principle” is however still intact and operating excellently. The creation of the α - and β -sheets⁷ as well as γ -sheets (this work) are byproducts and simple evidence for the validity of AP. It does not break down in any proposed formation. The hexagonal pattern (holes) in α -, β -, or γ -sheets, which can be considered as defects in triangular surfaces of nanostructures, improves the structure stability, as the impact of defects in crystalline.

Confirmations to the above predicted boron clusters and nanostructures come promptly. A series of theoretical and experimental studies appeared in consecutive years after 1994, confirming, in contrast to the 3D structures of bulk boron compounds, that boron clusters B_n with $n < 20$ prefer to be planar. Using *ab initio* quantum chemical approaches, Ricca and Bauschlicher³³ investigated small boron clusters B_n for $n = 2–14$ and substantiated that clusters for $10 < n < 14$ tend to possess quasi-planar structures. Li et al.^{34–37} investigated the structure and stability of neutral and charged small boron clusters B_n for $n = 4–8$ using similar theoretical methods. They found that the most stable isomers are in good agreement with those published by Boustani.³¹ Güvenç and co-workers investigated boron clusters B_n for $n = 2–12$ ³⁸ and recently B_n for $n = 13–20$ ³⁹ applying accurate *ab initio* quantum chemical and density functional methods. They found the same trend and consequently confirmed the quasi-planarity of boron clusters. Pandey et al.⁴⁰ presented a theoretical study of vibrational properties of neutral and cationic B₁₂ clusters based on density functional theory. They found that the ground state of these clusters exhibits geometries with convex and quasi-planar structures. They suggested that multicentered bonds together with delocalized charge density are dominant factors for the two-dimensional (2D) over three-dimensional (3D) configuration of these clusters. The calculated vibrational frequencies lie in the range 200–1328 cm^{−1}.

Further theoretical studies on boron clusters, particularly on cationic B₁₃, were carried out on the basis of different *ab initio* quantum chemical approximations and basis sets.^{41–43} Fowler and Ugalde⁴⁴ were the first who connected the stability and low reactivity of B₁₃⁺ with the aromaticity generated by the delocalization of π -electrons of the filled molecular orbitals. They asserted that this special stability was due to the aromatic

character of the quasi-planar cluster, similar to benzene. Furthermore, both B₁₂ and B₁₃⁺ clusters were studied by Kiran et al.⁴⁵ They found that the unusual stability of these clusters was due to the existence of multiple $4n + 2$ sextets. The H–L gaps in these planar and quasi-planar boron clusters depend on the nature of the interacting units and not just the π -electron count alone. Ahira et al.⁴⁶ established the aromaticity of planar boron clusters in terms of topological resonance energy. The latter two papers showed that the aromaticity concept is as useful in boron chemistry as it is in general organic chemistry. In addition, the structures of B₇, B₁₀, and B₁₃ clusters were studied by Cao et al.⁴⁷ using a full-potential linear-muffin-tin-orbital molecular dynamics method. They approved the “Aufbau principle” and the unique quasi-planarity of boron clusters. They mentioned that this principle is very useful in describing the growth of boron clusters.

The first experimental evidence of the quasi-planarity for boron clusters between B₁₀ and B₁₅ was recently presented by Wang et al.⁴⁸ combining photoelectron spectroscopy (PES) of size-selected anions with *ab initio* calculations. The boron cluster anions were produced by laser vaporization. Then they were entrained in a helium carrier gas and underwent a supersonic expansion to form a collimated cluster beam. The negatively charged clusters were analyzed with a time-of-flight mass spectrometer. The theoretical calculations on the anionic and neutral boron clusters were performed using (time-dependent) density functional theory and high quality basis sets. The authors provided that these boron clusters possess planar or quasi-planar structures. They asserted that the planarity is due to the delocalization of the π -electrons in 2D, which also renders aromaticity and antiaromaticity to the boron clusters analogous to planar hydrocarbons. They also found that electron deficiency of boron and the resulting multicenter bonding leave no dangling bonds in such 2D structures. In fact, Boldyrev, Wang, and co-workers initiated their theoretical and experimental investigations on neutral and charged boron clusters starting at B₃ and going toward B₈.^{49–53} They summarized and analyzed all of their obtained results on boron clusters and addressed that all boron aromatic clusters are potential new inorganic ligands and building blocks in chemistry.⁵⁴

In the current paper, we will study the geometric and electronic structures of boron nanoclusters with different morphologies as well as α -B₁₂ and γ -B₂₈ boron solids using *ab initio* quantum chemical and density functional theoretical methods. We will follow two kinds of calculations. The first kind is the noninteracting free-standing nanosystems like sheets, spheres, nanotubes, and elemental nanoscaled units of solid α -B₁₂ and γ -B₂₈ boron. These systems are mostly composed of up to 120 boron atoms. The other kind of calculations is for infinite systems underlying periodic conditions like staggered boron double-rings, nanosheets, and finally α -B₁₂ and γ -B₂₈. The considered periodic unit cells consist of a diverse number of atoms. The calculations will be carried out with different methods, potentials, and functionals using various program codes like Gamess_UK, Gaussian 03, VASP, and CPMD. The results will be presented for periodic systems and for free-standing nanoclusters of definite sizes, reflecting the reliability of the applied potentials and functionals in comparison with the experimental data. We will focus on the stability of clusters of the same size and show how some predicted structures compete with those originally belonging to solids. The paper is organized as follows: the computational methods will be described, and then, we will discuss the results starting at boron solids and going through sheets, spheres, rings, and nanotubes. The

structural transition and related stability will be presented and then finally the summary and conclusions.

II. Computational Methods

The theoretical basis for the current calculations are accurate *ab initio* methods for solving the many-electron problem of atoms, clusters, and solids. All-electron calculations were carried out in the frame of Hartree–Fock (HF) self-consistent-field (SCF) and density functional theory (DFT).^{55,56} Due to the number and size of the cluster systems (around 100 atoms), viewed in this work, we have considered the small basis set STO-3G. We are aware of the limitation of the STO-3G basis set, and we have used it to get a qualitative guidance about the stability of the systems. A higher quality basis set is likely to increase the stability of the system predicted by the STO-3G set. After assigning the point group symmetry, only a reasonably small set of parameters were left to be optimized, keeping the symmetry. The linear search for the local minima on the potential energy surfaces was carried out with the help of quasi-Newton search algorithms based on the knowledge of analytical gradients provided by the *ab initio* calculations. Due to the overwhelming number of basis functions (five per atom), some calculations were feasible only after applying the direct-SCF procedure, which computes integrals at each electronic iteration step. An optimization procedure was employed for the ground state, the restricted Hartree–Fock (RHF) procedure for closed-shell systems and the unrestricted Hartree–Fock (UHF) one for open-shell systems. The computed gradient-corrected exchange-correlation energy was based on density functionals (B3LYP) related to Becke (exchange)⁵⁷ and Lee, Yang, and Parr (correlation).⁵⁸ These concepts are some kernels of the used program packages Gamess_UK⁵⁹ and Gaussian 03.⁶⁰

Energetics, band structures, and density of states (DOS) of the periodic α -, γ -, and buckled-sheets as well as α -B₁₂ and γ -B₂₈ solids are investigated using the Vienna *ab initio* simulation package (VASP, version 4.6.31).^{61,62} This code is based on an iterative solution of the Kohn–Sham equations of the DFT using plane-wave basis sets and a supercell approach to model solid materials, surfaces, or clusters.⁶³ For boron sheets, where these systems should effectively be 2D monolayers, we were choosing a large vacuum distance (e.g., 10 Å) at the third direction to eliminate the interactions between layers. Two kinds of infinite sheet unit cells, namely, unit cell and supercell approaches, are used to compare the relative stabilities of these sheets and to investigate the effect of the unit cell size on the stability trend. The number of atoms in these unit cells for buckled-, α -, and γ -sheets are 2, 8, and 5 and 72, 72, and 80 for the unit cell and supercell approaches, respectively (Table 2).

It is observed that the trend for the stability is the same for these two approaches. In the DFT calculations, we have considered the local density approximation (LDA) as well as the exchange-correlation interactions, approximated by the generalized gradients approximation (GGA) with the Perdew–Wang parametrization (PW91).^{64,65} The projected augmented wave (PAW) method^{66,67} was used. The GGA/PW91 method was employed self-consistently for optimizations of the structures and obtaining energetics and non-self-consistently for the DOS and band structure calculations. For the k -point sampling of the Brillouin zone, Monkhorst–Pack was used and also a default value for the Fermi smearing width of 0.2 eV was applied. The optimal sizes of the k -point meshes for different systems were individually converged, such that changes in the total energy were reduced to less than 10 meV. The procedure

TABLE 1: Atoms/Cell, Monkhorst–Pack (K -Points), Cutoff, Band Gap, and Binding Energy per Atom E_b /Atom of α -B₁₂ and γ -B₂₈ Solids, Obtained at the GGA/B3LYP and TMP (CPMD), GGA/PW91 and PAW (VASP) Levels of Theory^a

system	atoms/ cell	Monkhorst– Pack	cutoff	E_b / atom	band gap
Experimental					
α -B ₁₂				6.00 ⁷⁴	2.0 ^{75,76}
γ -B ₂₈					2.1 ³⁰
CPMD					
α -B ₁₂ -periodic ^b	12	4 × 4 × 4	680	5.98 ^d	2.06 (1.66) ^f
γ -B ₂₈ -periodic ^c	28	4 × 4 × 4	680	5.94 ^d	2.08 (1.87) ^f
VASP					
α -B ₁₂ -periodic	12	6 × 6 × 6	398.3	6.686 ^e	2.65 (1.50) ^f
γ -B ₂₈ -periodic	28	10 × 9 × 8	398.3	6.659 ^e	2.50 (1.63) ^f

^a The cutoff, E_b /atom, and band gap are given in eV. ^b α -Boron lattice constants: $a = 5.04$ Å, $\alpha = 58.5^\circ$ (Figure 1). ^c γ -Boron optimized lattice parameters: $a = 5.04$ Å, $b = 5.62$ Å, and $c = 7.01$ Å. ^d E_b /atom = $E_{\text{B-atom}} - E_{\text{Solid}}/n$, where n is the number of atoms/cell. ^e E_b /atom = E_{Solid}/n , where n is the number of atoms/cell. ^f The direct and indirect (in parentheses) band gaps.

for obtaining these optimal sizes and also the other details related to the applied stages/calculations with VASP can be found in ref 68.

Further calculations on α -rhombohedral and γ -orthorhombic boron were performed by using the CPMD code, version 3.13.2.^{69,70} This code is also based on the DFT with plane waves and pseudopotentials.^{55,56,71} The norm-conserving Troullier–Martins-type pseudopotentials (TMP)⁷² were used. The generalized gradient approximation (GGA) was included by means of the functional (B3LYP) derived by Becke⁵⁷ and by Lee, Yang, and Parr.⁵⁸ An energy cutoff of 50 Ry (680 eV) for the plane-wave expansion was sufficient to provide a convergence for total energies and geometries. We have already confirmed in a previous work that the total energies converged at a smaller cutoff of 40 Ry for this pseudopotential. Because the unit cell is large, k -point sampling in the total energy calculation was performed by using Monkhorst–Pack sampling⁷³ of a (4 × 4 × 4) mesh. The results were compared with those of a finer mesh, and it was found that the difference in the total energy per atom was less than 6×10^{-4} eV. Since the reference energy of α -rhombohedral solid boron is determined at zero temperature and zero pressure, then all calculations will be carried out at zero temperature and zero pressure also.

III. Results and Discussion

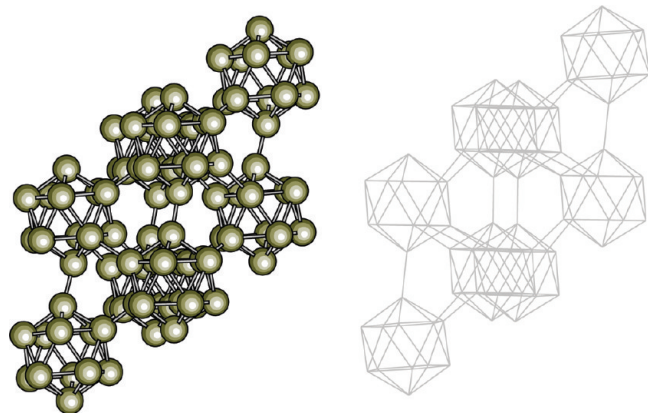
In the current work, we are running two kinds of calculations. The first kind is the free-standing noninteracting nanoclusters in the form of rings, spheres, and sheets of different sizes, and of course the elemental unit cells of α -rhombohedral (α -B₁₂) and γ -orthorhombic (γ -B₂₈) boron. The second kind of calculations are those structures underlying periodic interacting conditions, representing infinite systems like the staggered double-rings, α - and γ -sheets, or α -B₁₂ and γ -B₂₈ solids. Due to the fact that the α -rhombohedral boron is a real existing solid and the most well-known one under boron solids, it is evident and meaningful to consider its measured cohesive energy as a reference for all obtained energies of boron clusters and solids. The α -rhombohedral boron cluster consists of eight icosahedra 8 × B₁₂, whose centers are located on each of the corners of the rhombohedron, as shown in Figure 1.

We define the stability of the clusters, calculated at the HF-SCF and B3LYP levels of theory (Gaussian and Gamess_UK), through the binding energy per atom as E_b /atom = $E_{\text{B-atom}}$ –

TABLE 2: The Binding (Cohesive) Energy per Atom E_b/Atom of Periodic Boron Sheets, Obtained at the LDA, GGA/PW91, and PAW Level of Theory (VASP)

system	cell size (Å)	atoms per cell	Monkhorst–Pack K-points	cutoff (eV)	E_b/atom (eV)
		GGA (VASP)			
Buckled-sheet ^a	$1.6 \times 2.91 \times 10$	2	$11 \times 7 \times 5$	398.3	6.197 ^d
α -sheet ^b	$5.06 \times 5.06 \times 10$	8	$9 \times 9 \times 4$	398.3	6.300 ^d
γ -sheet ^c	$5.06 \times 2.93 \times 10$	5	$5 \times 17 \times 3$	398.3	6.259 ^d
		LDA (VASP)			
Buckled-sheet ^a	$9.85 \times 17.06 \times 10.0$	72	$3 \times 3 \times 3$	435	6.316 ^e
α -sheet ^b	$7.46 \times 12.92 \times 0.0$	72	$2 \times 2 \times 2$	435	6.402 ^e
γ -sheet ^c	$20.01 \times 11.55 \times 10.0$	80	$3 \times 3 \times 3$	435	6.330 ^e

^a The buckled-sheet (Figure 4, upper). ^b The precursor α -sheet (Figure 3, lower) of the B₈₀ cage, proposed by Yakobson et al.⁸ ^c The precursor γ -sheet (Figure 3, upper) of the B₁₀₀ cage, proposed by Mukhopadhyay et al.¹¹ ^d $E_b = E_{\text{Sheet}}/n$, where n is the number of atoms/cell. ^e $E_b = E_{\text{B-atom}} - E_{\text{Sheet}}/n$, where n is the number of atoms/cell.



B₉₆ as rhombohedral α -Boron

Figure 1. The α -B₁₂ rhombohedral solid boron cell is composed of eight icosahedra $8 \times \text{B}_{12}$, whose centers are located on each of the corners of the rhombohedron.

E_{cluster}/n , where E_{atom} is the energy of a single boron atom, E_{cluster} is the final energy of the calculated boron cluster, and n is the number of atoms in the cluster. The cohesive energy of the γ -B₂₈ solid, obtained at the GGA/PW91 and PAW (VASP), is defined as $E_b/\text{atom} = E_{\gamma\text{-B}_{28}}/n$, where $E_{\gamma\text{-B}_{28}}$ is the energy of the unit cell and n is the number of atoms per cell. Hereafter, the calculated cohesive or the binding energy per atom (E_b/atom) of α -rhombohedral boron generated by the periodic icosahedral unit B₁₂ was obtained at different theoretical levels. At the B3LYP/STO-3G level (Gaussian 03), it is about 7.66 eV (Table 3), at the GGA/PW91 and PAW (VASP) levels, about 6.68 eV, and at GGA and TMP (CPMD), about 5.98 eV (Table 1). In comparison, the experimental value of the solid α -rhombohedral boron is about 6.0 eV.⁷⁴ The calculated E_b/atom of an infinite boron strip of a double-ring, obtained at the B3LYP/STO-3G level of theory (Gaussian 03), is about 6.782 eV (Table 3).

The calculated direct band gaps of α -rhombohedral and γ -orthorhombic boron, obtained at the GGA/B3LYP and TMP levels (CPMD), are 2.06 and 2.08 eV, respectively. The measured band gaps of both solids α -rhombohedral and γ -orthorhombic boron are, respectively, 2.0 eV^{75,76} and 2.1 eV³⁰ (Table 1). It is certain that these experimental values will be considered as the reference values for the current theoretical calculations of solids. The calculated value of the infinite boron strip is considered as the reference energy for all free-standing noninteracting clusters, being the B₉₆ isomers, sheets, spheres, multiring, and quasi-planar systems, or the noninteracting cells of α -rhombohedral and γ -orthorhombic boron, considered in the current work.

TABLE 3: The Binding Energy per Atom E_b/Atom of Boron Clusters and of the Periodic Systems: The Infinite Strip and Solid α -Boron^a

group	structure	symmetry	E_b^{SCF} eV	E_b^{B3LYP} eV
icosahedral	$\text{B}_{96}(8 \times \text{B}_{12})_{\text{Rh}}$ ^b	C_i	4.755	6.366
	$\text{B}_{96}(8 \times \text{B}_{12})_{\text{Ring}}$ ^c	C_{8v}	4.667	6.293
	$\text{B}_{120}(9 \times \text{B}_{12} + 6 \times \text{B}_2)$ ^d	C_{2h}	4.696	6.245
multirings	$\text{B}_{96}(2 \times 48)$	D_{48d}	5.327	6.774
	$\text{B}_{96}(3 \times 32)$	D_{32h}	5.267	6.786
	$\text{B}_{96}(4 \times 24)$	D_{24d}	5.069	6.676
	$\text{B}_{96}(6 \times 16)$	D_{16d}	4.927	6.562
	$\text{B}_{96}(8 \times 12)$	D_{12d}	4.660	6.411
	$\text{B}_{96}(3 \times 16 + 2 \times 24)$ ^e	C_{8v}	5.087	6.451
	$\text{B}_{120}(3 \times 40)$ ^f	D_{40h}	5.264	6.790
	$\alpha\text{-B}_{96}^g$	C_{2h}	4.695	6.328
sheets	$\gamma\text{-B}_{96}^h$	D_{2h}	4.759	6.385
	planar-B ₉₆	C_{2h}	4.684	6.376
spheres	buckled-B ₉₆	C_1	4.828	6.429
	B_{80}^g	I_h	5.220	6.737
	B_{96}	C_{2h}	5.202	6.705
periodic	B_{100}^g	C_{2h}	5.318	6.809
	α -boron	C_i	6.419	7.660
	strip ⁱ	C_1		6.782

^a The calculations were carried out at the HF-SCF and B3LYP levels of theory using the STO-3G basis set (Gaussian 03, Gammes_UK). ^b The rhombohedral cell of α -boron (Figure 1). ^c The ring of icosahedra (Figure 5). ^d The B₁₂₀ γ -boron cluster (Figure 2). ^e The double-walled rings (Figure 5). ^f The B₁₂₀ triple-ring cluster (not shown), the counterpart to the B₁₂₀ γ -boron cluster. ^g The precursor α -sheet of the B₈₀ cage (Figure 3) proposed by Yakobson et al.⁸ ^h The precursor γ -sheet of the B₁₀₀ cage (Figure 3) proposed by Mukhopadhyay et al.¹¹ ⁱ The infinite strip, optimized for the dimer B₁ (0,0,0,0,0) and B₂ (0.79289,1.52501,0,0) with the translation vector TV(1.5858,0,0,0).

1. Solid Boron α -B₁₂ and γ -B₂₈. Before we present our contribution to γ -B₂₈ solid, we refer to one of the most important properties of this phase, namely, its hardness. In comparison to the Vickers hardness H_V values 42 and 45 GPa of α -B₁₂ and β -B₁₀₆,⁷⁷ respectively, the corresponding H_V value of γ -B₂₈ rises to 50 GPa⁷⁷ or to 58 GPa.³⁰ Thus, this new high-pressure phase γ -B₂₈ has the highest hardness among the known boron crystallines. In addition, the H_V value, determined by Zarechnaya et al.,³⁰ is in the range of polycrystalline cubic boron nitride (cBN) that makes γ -B₂₈ the second hardest elemental solid after diamond. Furthermore, Jiang et al.⁷⁸ determined via first-principles calculations some mechanical properties of γ -boron like bulk and shear modulus, Young's moduli, and Poisson's ratio. They confirmed that γ -B₂₈ can be a superhard material. They also found that this material possesses a similar bulk modulus to B₆O and a shear modulus that is 16% higher.

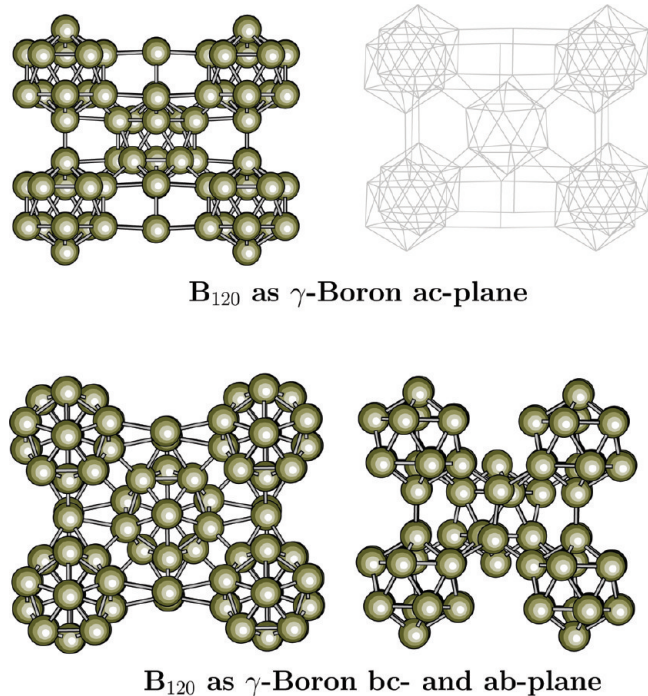


Figure 2. The B₁₂₀ ($9 \times B_{12} + 6 \times B_2$) cluster, as a cut of the γ -B₂₈ orthorhombic solid boron, is composed of nine boron icosahedra and six boron pairs, viewing the perspective of the planes ac, bc, and ab.

Oganov et al.¹ found that the average intraicosahedral bond length is 1.80 Å and that of the pairs is 1.73 Å.

Oganov et al.¹ claimed that the charge transfer between the constituent clusters makes the γ -B₂₈ a boron boride (B_2) ^{$\delta+$} (B_{12}) ^{$\delta-$} so that the B₂ pairs and B₁₂ icosahedra are acting as anions and cations, respectively. In contrast, the experimental single-crystal structural data of Zarechnaya et al.³⁰ and their theoretical results do not confirm Oganov's model. In other words, the ionic boron boride remains a controversial issue.^{79,80} However, in our GGA/PW91 and PAW (VASP) unit cell calculations, the charge transfer between the constituent clusters of γ -B₂₈ was about $\delta = 0.2125$, obtained from the Bader decomposition of charge density, determined after the algorithm of Henkelmann et al.⁸¹ In addition, the Mulliken charge distribution of our B₁₂₀ ($9 \times B_{12} + 6 \times B_2$) cluster model for solid γ -B₂₈, achieved at the B3LYP/STO-3G level (Gaussian 03), shows a charge transfer between the six dimers and the nine icosahedra ($6 \times B_2$) ^{$\delta+$} ($9 \times B_{12}$) ^{$\delta-$} . The average charge transfer is about $\delta = 0.39$, obtained as the sum of charges localized at the dimers or the icosahedra. Thus, we confirm Oganov's results that γ -B₂₈ has an ionic character.

The calculated E_b /atom of periodic γ -B₂₈ boron (Figure 2) is about 6.659 eV obtained at the GGA/PW91 and PAW (VASP) levels (Table 1). It is about 27 meV less stable than α -B₁₂ rhombohedral boron (Figure 1). Consistent with the E_b /atom value of γ -B₂₈ boron, 5.94 eV, calculated at the GGA/B3LYP and TMP (CPMD) levels, it is about 40 meV less stable than α -B₁₂ (Table 1). The trend that α -B₁₂ is more stable than γ -B₂₈ at zero temperature and pressure is consistent in both methods, confirming the enthalpy results of Oganov et al.¹ This statement becomes a further confirmation by the clusters. The B₁₂₀ ($9 \times B_{12} + 6 \times B_2$) cluster (Figure 2), which is a cut of γ -B₂₈ boron and composed of nine icosahedra and six pairs, is energetically by 545 meV less stable than the triple-ring B₁₂₀ (3×40), a cluster of the same size (Table 3). The B₁₂₀ ($9 \times B_{12} + 6 \times B_2$) cluster is rather 121 meV less stable than the rhombohedral cell

B₉₆ of α -boron. Thus, the cluster calculations support the CPMD and VASP calculations. In comparison with the experimental cohesive energy of α -boron, the calculated value 5.98 eV, obtained with the methods considered by the CPMD code, seems to be in excellent agreement with the experimental value 6.0 eV⁷⁴ and also more reliable than that obtained with the methods considered by the VASP code. The latter one is about 6.69 eV and nearly 11.4% larger than the experimental value. Therefore, the GGA/B3LYP and TMP potentials (CPMD) are for boron solids more reliable than the GGA/PW91 and PAW (VASP) ones.

2. Boron Sheets. Following the Aufbau principle, we extended quasi-planar and convex boron clusters to build up sheets, nanotubes, and spheres. Highly stable small boron fragments of sheets B_n for $n = 10$ to 16, 20, 22, 32, 42, and 46⁴ were constructed. Due to the fact that these boron sheets are the precursors for boron nanotubes, few studies were dedicated to the identification and characterization of boron sheets.^{82–84} The most stable structure for boron sheets was predicted to be triangular, mainly consisting of dovetail hexagonal pyramids with the pyramidal tips up and down, thus a boron surface with a buckled character. This buckling in boron sheets was confirmed by all authors mentioned above. The unique property of these boron sheets is their electronic conductive character in contrast to the semiconductor α -boron which has a band gap of 2.0 eV (Table 1).

One of the most important studies on boron sheets was carried out by Lau and Pandey⁸⁶ using *ab initio* first-principles methods. They investigated systematically the stability, morphology, and electronic properties of several sheet configurations and found that those of triangle composed sheets exhibit the highest stability, in complete agreement with our predictions.^{4,6} Further improvement to the stability of boron sheets was recently suggested by Tang and Ismail-Beigi⁷ and Yang et al.⁸⁷ They proposed new sheets (α -sheet) which can be obtained by removing atoms from flat triangular sheets. Each removal produces a hexagonal hole (defect) and releases a mixture of hexagons and triangles. This mixture should place the Fermi energy exactly at the zero point of in-plane projected densities of states, filling all available in-plane bonding states and none of the antibonding ones. They found that these boron sheets are metallic and can be rolled up into nanotubes. A further study on boron sheets was carried out by Lau and Pandey⁸⁸ using again first-principles methods based on DFT to calculate the thermodynamic properties of several configurations of the pristine 2D sheet. They found that the thermodynamical stability of boron sheets is predicted to be composed of a hybrid of triangular and hexagonal configurations.

Besides the above-mentioned α -sheet (Figure 3, lower) and the triangular sheet (Figure 4), each composed of 96 atoms, we propose a sheet with the same atomic size, called the γ -sheet (Figure 3, upper). It is decorated similarly to the α -sheet but with parallel hexagonal holes. We have calculated these three configurations first as free-standing noninteracting clusters applying the HF-SCF and B3LYP methods using the standard basis set STO-3G and then as periodic systems of infinite sheets with the corresponding unit cells by different numbers of atoms per cell. The first set of periodic system calculations was carried out for 2, 8, and 5 atoms per cell applying the GGA/PW91 and PAW methods (VASP) and the next set for 72, 72, and 80 atoms per cell applying the LDA and PAW methods (VASP), with respect to the buckled-sheet, α -sheet, and γ -sheet. As a free-standing cluster, the B3LYP calculations show that the triangular sheet with E_b /atom = 6.42 eV (Table 3) was more stable than

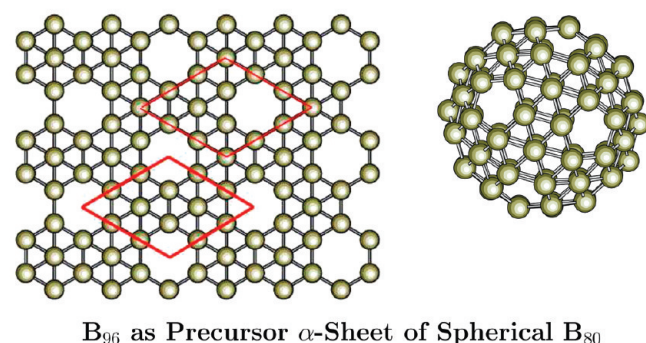
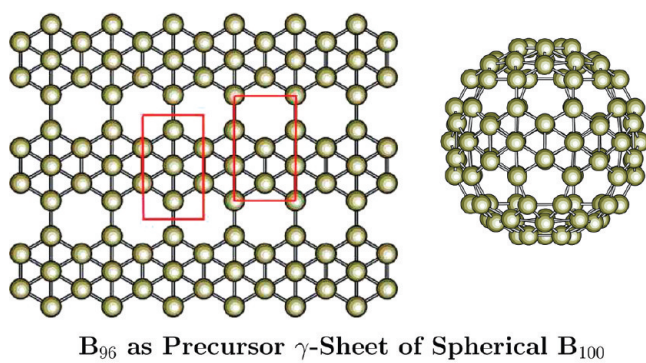


Figure 3. The B₉₆ clusters as precursors for the γ -sheet of the B₁₀₀ sphere (upper) and for the α -sheet of the B₈₀ sphere (lower).

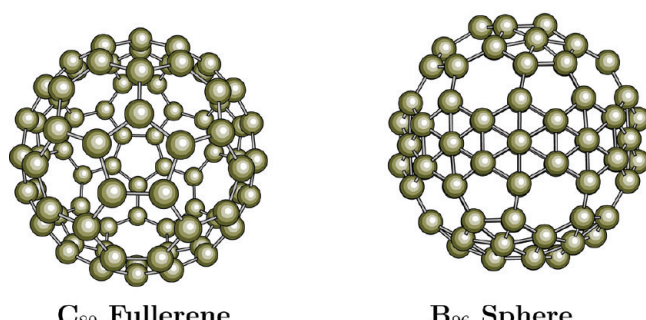
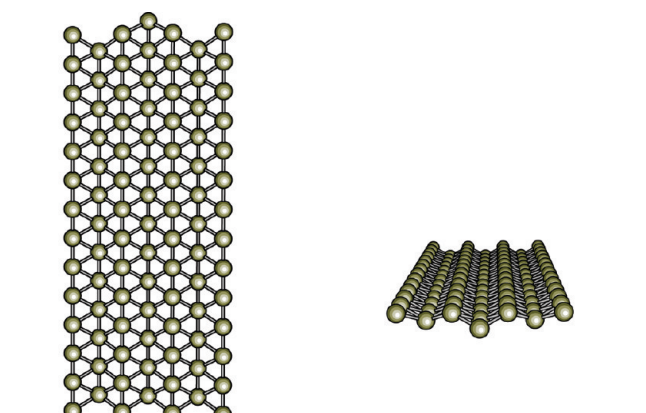


Figure 4. The B₉₆ cluster of the buckled-sheet with a side perspective (upper). The carbon C₈₀ fullerene (lower left) as a scaffold for generating the boron B₉₆ sphere (lower right).

the α -sheet and γ -sheet by 101 and 44 meV, respectively. In contrast, in the periodic systems, the α -sheet with E_b/atom values of 6.30 and 6.40 eV, obtained for 8 and 72 atoms/cell, respectively, is the most stable infinite sheet followed by the γ -sheet and triangular sheet (Table 2). Independent of the

considered number of atoms/cell in VASP calculations, we confirm herewith the results of Tang and Ismail-Beigi⁷ that the α -sheet as an infinite system is the most stable configuration of sheets. However, further quantitative calculations are required to verify our finding.

3. Spherical and Icosahedral Boron Clusters. Small pure boron spheres were predicted by Boustani.⁸⁹ He constructed spherical boron clusters B₁₂, B₂₂, B₃₂, and B₄₂ according to the Aufbau principle as dovetail pentagonal and hexagonal pyramids. Ten years later follows a series of papers studying spherical boron structures. B₈₀ fullerenes were presented by Yakobson and co-workers.^{8,9} On the basis of first-principles methods, they generated spherical boron cages as a combination of several staggered double-rings crossing together with a rhombus. The energies of the generated spheres were compared with the corresponding reference energies of the double-rings. They found that B₈₀ (Figure 3, lower) was the most stable sphere symmetrically similar to the structure of the buckyball C₆₀. The only difference is the presence of an additional atom at the center of each hexagon. These facets of the B₈₀ follow the Aufbau principle, although the hexagonal pyramid units here are rather planar. Jemmis et al.¹⁰ showed via first-principles study that stuffed spherical boron clusters B_n for n = 98–102 are more stable than fullerene-like boron clusters. By means of *ab initio* and DFT calculations, Su et al.⁹⁰ presented solid B₈₀ in a fcc structure. They found that the B₈₀ cages are geometrically distorted, while boron–boron chemical bonds are formed between every two nearest neighbor B₈₀ cages. Lui et al.⁹¹ carried out a density functional theoretical investigation of bcc B₈₀ and K₆B₈₀, showing that B₈₀ can condense into stable solids closely on a bcc lattice. B₈₀ is more stable in the fcc structure, and the stability in bcc can be enhanced through interaction with potassium. Su et al.⁹² generated a family of boron fullerenes and proposed a general constructing scheme and electron counting based on *ab initio* calculations.

A recent *ab initio* study on spherical boron clusters B_n for n = 12–122 was presented by Mukhopadhyay et al.¹¹ They considered the energies of the double-ring boron structures as reference energies to those of spherical structures with the corresponding cluster size. They found that the most stable sphere is made up of 100 atoms (Figure 3, upper) which is more stable than the counterpart the double-ring B₁₀₀ and even by 72 meV more stable than the B₈₀ proposed by Yakobson et al.^{8,9} The structure of the B₁₀₀ sphere was generated from the carbon C₈₀ fullerene (Figure 4, lower left), composed of 12 pentagons and 30 hexagons, by setting boron atoms to 20 centers of 30 hexagons of the polyhedron and counting 10 hexagonal holes. The precursor sheet of the spherical B₁₀₀ cluster exhibits parallel holes each characterized by six surrounding atoms. Similarly, the Yakobson cage B₈₀⁸ was generated from the C₆₀ fullerene by setting boron atoms to the centers of the 20 hexagons. The precursor sheet of the B₈₀ fullerene (Figure 3, lower) is nothing else than the α -sheet of Ismail-Beigi.⁷

Larger spherical boron fullerenes were proposed by Szwacki⁹³ using first-principles methods. These fullerenes have similar structures consisting of six interwoven boron double-rings. He proposed B₈₀, B₁₈₀, and B₃₀₀ cages, and each is accompanied by its precursor sheet. He found that the most stable fullerene is made up of 180 atoms, has almost a perfect spherical shape, and is more stable than the B₈₀ fullerene by 10 meV. These sheets have atomic motifs with C_{3v} symmetry, similar to the quasi-planar B₇, B₁₂, and B₁₈ clusters. The precursor sheets of B₈₀, B₁₈₀, and B₃₀₀ exhibit holes characterized, respectively, by 6, 9, and 12 surrounding atoms. Much larger boron fullerenes

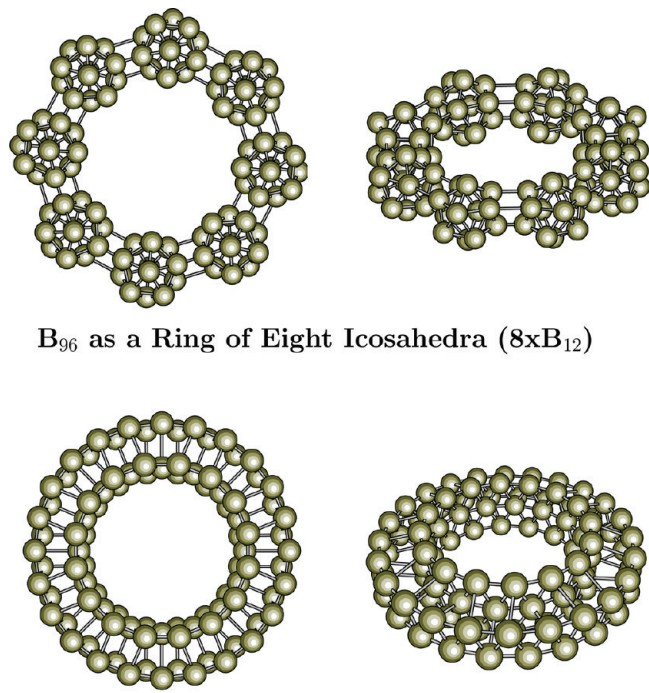


Figure 5. The B_{96} cluster as a ring of eight icosahedra ($8 \times B_{12}$) with a side perspective (upper). The B_{96} cluster as double-walled rings ($3 \times 16 + 2 \times 24$) where the atoms of the inner wall are matching with atoms of the outer wall.

were proposed by Zope et al.,⁹⁴ demonstrating the existence of a boron family containing $80n^2$ atoms for $n = 1–5$ in relation to the family of $60n^2$ carbon icosahedral fullerenes. The fullerenes $B_{1280}–B_{2000}$ ($n = 4–5$) become metallic, while their $60n^2$ carbon cousins are semiconductors. Furthermore, Zope⁹⁵ proposed hollow boron spheres which can be obtained using six four-member rings instead of 12 pentagonal rings in boron fullerenes. One of these hollow spheres, in which pentagons were replaced by squares, particularly the B_{32} sphere, was already reported by Boustani et al.⁹⁶

A new spherical cluster B_{96} (Figure 4, lower right) is proposed in the current work. The structure of the B_{96} sphere was also generated from the C_{80} fullerene (Figure 4) by setting boron atoms only to 16 centers of 30 hexagons of the polyhedron C_{80} and counting four hexagonal holes more than the spherical B_{100} . As can be seen in Table 3, the B_{96} sphere is by 32 and 104 meV less stable than the B_{80} and B_{100} spheres, respectively, while B_{80} is about 72 meV less stable than the B_{100} sphere. Recent B3LYP-DFT/6-31G* calculations on B_{80} and B_{100} fullerenes were carried by He et al.⁹⁷ They found that the B_{100} sphere is by 10 meV/atom more stable than the B_{80} fullerene. Therefore, the spherical B_{100} cluster remains the most stable one between the spheres. The average diameters of these three cages B_{80} , B_{96} , and B_{100} are, respectively, 6.72, 10.78, and 10.86 Å. Another B_{96} isomer was constructed by eight icosahedra distributed and connected to each other along a ring (Figure 5, upper). Each icosahedron is connected with the next neighbor by three covalent bonds. In comparison with the icosahedral arrangement of α - B_{12} boron, in which the centers of the eight icosahedra are located on each of the corners of the rhombohedron, it seems the ring of the eight icosahedra $B_{96}(8 \times B_{12})$ is less favorable energetically. It is by 73 meV less stable than the rhombohedral unit of α - B_{12} boron. However, the spherical clusters B_{80} , B_{96} , and B_{100} are more stable than both icosahedral arrangements.

4. Multiring Systems toward Nanotubes. It was shown that folding of boron sheets into nanotubes occurs over an energy barrier and that the larger the diameters the more stable the nanotubes are.⁸⁵ Like sheets, boron nanotubes were found to be electrically conductive.⁶ A recent study ascertained that the conductivity of boron nanotubes is independent of their chirality,⁹⁹ contrary to carbon nanotubes. Boron nanotubes were also explored by several groups showing that the armchair and zigzag boron nanotubes are characterized with a buckling surface.^{83,84} Evans et al.⁸² confirmed that (n,n) nanotubes that arise from the buckled plane have lower curvature energies than the $(n,0)$ tubes arising from the triangular plane. Furthermore, Lau et al.¹⁰⁰ studied the stability, morphology, and electronic properties of boron nanotubes using the periodic DFT. The presence of the directional σ -type interactions with the delocalized π -type ones appears to stabilize the sheets. However, boron nanotubes formed by wrapping the reconstructed sheet are predicted to be metallic due to a curvature-induced transition in the electronic properties. Additional investigation on the mechanical and electronic properties of (with holes) decorated boron nanotubes was carried out by Singh et al.¹⁰¹ by folding the boron α -sheets. They generated the so-called boron α -tubes which have been proposed at the same time by Yang et al.⁸⁷

Furthermore, double-walled boron nanotubes (DWBNTs) were proposed and investigated in a recent study performed by Sebetci et al.¹⁰² using first-principles methods based on DFT. The structure of the DWBNTs is two single-walled boron nanotubes (SWBNTs) one inside the other. The puckering of the boron sheets allows the inner atoms of the outer wall and outer atoms of the inner wall to be matched, giving the sp-type hybrid a bonding between the walls. This matching was in fact a bond interaction between the walls in the form of σ -bonds. These covalent bonds between the double walls are in contrast to those of the carbon nanotubes where the walls are connected by van der Waals forces only in which no chemical bonds are formed among the neighboring walls. The density of states of both zigzag and armchair DWBNTs indicates that they are metallic. The most stable one among all studied DWBNTs is an armchair DWBNT with a C_6 rotational symmetry. Further first-principles study on crystalline bundles of SWBNTs was presented by Pandey et al.¹⁰³ They have shown that these structures are thermodynamically stable due to the dominance of the intertubular interactions involving two-centered and three-centered bonding features in the SWBNT bundles. A subtle competition between the intra- and intertubular bonds appears to lead to polymorphism associated with boron nanotubes, suggesting that it may be one of the causes of the difficulty in synthesizing SWBNTs. The experimental evidence of the SWBNTs was declared (2004) by Ciuparu et al.,¹⁰⁵ which were predicted (1997).³² They reported the first synthesis of pure boron nanotubes by reaction of boron trichloride with hydrogen over a magnesium-substituted mesoporous silica template Mg-MCM-41 catalyst with parallel, uniform-diameter (36 ± 1 Å) cylindrical pores. The presence of tubular structures has been confirmed by the presence of spectral features in the Raman breathing mode region at wavenumbers below 500 cm^{-1} . The boron nanotubes have diameters of approximately 3 nm and a measured length of about 15–20 nm outside the pores of the catalyst.

The multiring system (Figures 6 and 7), consisting of double-, triple-, quadruple-, sextuple-, and octuple-rings with different diameters, is the key to understanding the development and emerging of the nanotubes at the outset phase. As to be seen in Table 3, the average B3LYP value of the stability (E_b/atom) of

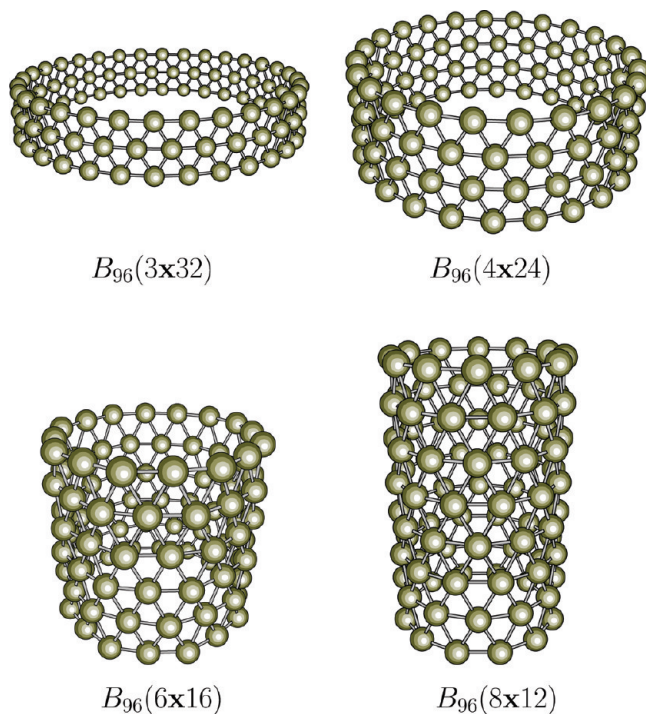


Figure 6. The isomers of B_{96} clusters presented in clockwise: triple-ring (3×32), quadruple-ring (4×24), sextuple-ring (6×16), and octuple-ring (8×12).

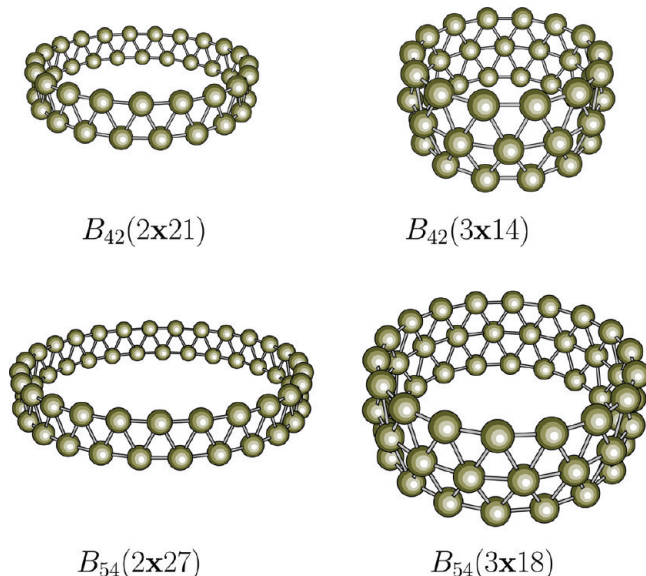


Figure 7. The clusters B_{42} presented as double-ring (2×21) and triple-ring (3×14) (upper). The B_{54} clusters, presented as double-ring (2×27) and triple-ring (3×18).

the multirings is close to that of the infinite strip. The narrowest nanotube $B_{96}(8 \times 12)$ with a diameter of 6.4 \AA and the double-walled multiring system $B_{96}(3 \times 16 + 2 \times 24)$ (Figure 5, lower) with an inner diameter of 8.4 \AA are about 371 and 331 meV less stable than the strip, respectively. The difference in stability of the middle-sized systems of $B_{96}(6 \times 16)$ of 8.4 \AA diameter and $B_{96}(4 \times 24)$ of 12.6 \AA diameter from the strip reduces to values of 220 and 106 meV. The finite double-ring $B_{96}(2 \times 48)$ with a diameter of 24 \AA is only by 8 meV less stable than its infinite counterpart, the strip. Just the stability of the triple-ring system $B_{96}(3 \times 32)$ with a diameter of around 16 \AA exceeds by only 4 meV the corresponding value of the strip. However, the stability of the triple-ring system $B_{120}(3 \times 40)$ with a

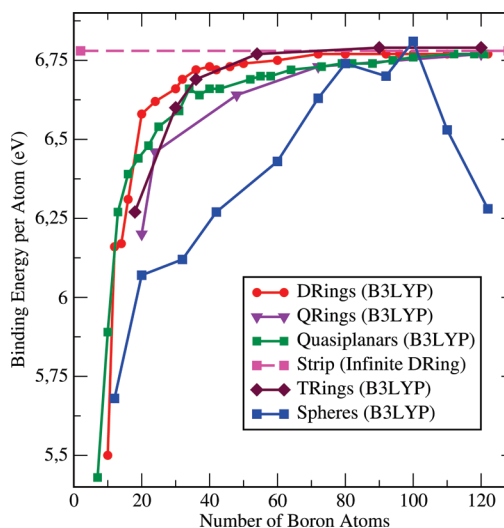


Figure 8. The stability of spherical, quasi-planar, double-ring, triple-ring, and quadruple-ring boron clusters as a function of the cluster size, obtained at the B3LYP level. The diagram shows the transition (crossing) from quasi-planar to double-ring (red and green) and then from double-ring to triple-ring (red and brown). It points out that the B_{100} sphere is the most stable structure, even more stable than the infinite strip.

diameter of 20 \AA is slightly (8 meV) above than that of the strip. Hereupon, one can ascertain that comparison of the stability of these multirings can give a simple relationship between the structures and their diameters: the larger the diameters, the more stable the multirings or rather the nanotubes. This consideration was already established by rather smaller nanotubes.⁸⁵

5. Boron Rings B_{2n} , B_{3n} , and B_{4n} . As a matter of fact, small multiring systems as precursors of boron nanotubes were reported by Boustani and Quandt³² for the first time. Multiring systems beginning by single-, double-, triple-rings and so forth were already studied for different sizes and numbers of boron rings like B_{24} ,⁹⁸ B_{32} ,⁹⁶ B_{36} ,³² and B_{96} .¹⁰⁴ According to these systems, the staggered double-ring armchair tubular boron cluster seems to have the largest E_b/atom and thus consequently the highest stability. Thereupon, Yakobson et al.^{8,9} and Mukhopadhyay et al.¹¹ considered the energies of finite and infinite double-ring systems as the reference energy for all 2D and 3D boron clusters. Recently, however, staggered triple-ring boron systems B_{3n} for $n = 8-32$ were systematically studied by Tian and Wang.¹⁰⁶ They found that triple-ring systems B_{3n} for $n = 14-32$ are more stable than the double- and quadruple-ring systems. The triple-ring does not favor sp^2 hybridization but can be composed of a simple up and down puckering model satisfying the Aufbau principle.

In the current work, we have studied the stability of the triple-ring system B_{3n} and the quadruple-ring system B_{4n} . Then, we compared it to the stability of the B_{2n} system obtained in a previous work.¹¹ The calculations were carried out at the B3LYP/STO-3G level of theory. The clusters of the triple-ring systems B_{3n} were considered for $n = 6, 10, 12, 18, 30$, and 40, while those of the B_{4n} system for $n = 5, 6, 12, 18$, and 30. The E_b/atom values of all of these clusters are displayed in Figure 8. In comparison with the corresponding E_b/atom of the spherical, quasiplanar, and double-ring systems, we find that the clusters of the triple-ring system B_{3n} , assigned by TRings, are more stable than the double-ring system for $n > 16$ and obviously more stable than the quadruple-ring system B_{4n} for all n . The E_b/atom of B_{3n} is also higher than the infinite strip of the double-ring by $n > 70$. Herewith, we confirm the results of

Tian and Wang¹⁰⁶ that the triple-ring system is the most stable ring system when $n > 14$. The structural transition from double-ring to triple-ring systems was properly investigated and explained in the previous section.

6. Structural Transition. Many topologies of boron nanostructures, like clusters, cages, sheets, rings, and nanotubes, were established theoretically and experimentally. The structures of small clusters up to a cluster size of 14 atoms were experimentally confirmed to be 2D or quasi-planar. Clusters of larger sizes, e.g., $n \geq 20$, were found to be 3D in the form of double-rings.^{96,98} A recent paper found that clusters of a size of $n \geq 40$ have three-membered rings.¹⁰⁶ Now the simple question arises: at which cluster size does the structural transition (ST) from planar to nonplanar forms or from two-ring to three-ring systems occur? Kiran et al.¹⁰⁷ have shown that experimental and computational simulations revealed that boron clusters, which favor planar 2D structures up to 18 atoms, prefer 3D structures beginning at 20 atoms. Using basin-hopping global optimization methods coupled with the *ab initio* DFT technique, they found that the B_{20} neutral cluster has a double-ring tubular structure with a diameter of 5.2 Å. For the B_{20} anion, the tubular structure is shown to be isoenergetic to 2D structures, which were observed and confirmed by photoelectron spectroscopy. The transition from 2D to 3D was observed at B_{20} , reminiscent of the ring-to-fullerene transition at C_{20} in carbon clusters, which suggests it may be considered as the embryo of the thinnest single-walled boron nanotubes.

Marques and Botti¹⁰⁸ examined the transition question from the optical point of view. They applied the time-dependent DFT using real time and space to solve the time-dependent Kohn–Sham equations. They have shown that the optical spectroscopy can be applied to distinguish without ambiguity between the different low-energy members of the B_{20} family. The most stable neutral B_{20} isomer is the tubular cluster which can be unequivocally identified due to the presence of a very sharp resonance at about 4.8 eV. The transition from 2D to 3D and chemical bonding in elemental boron nanoclusters were studied by Lau and Pandey.¹⁰⁹ They asserted that, in both the small-cluster regime of $n \leq 20$ and the large-cluster regime of $n \geq 20$, the preferred topological structures are the result of the interplay between bonding factors related to the delocalized π -bonds and the intericosahedral and intraicosahedral bonds. Furthermore, An et al.¹¹⁰ studied the relative stability among four low-lying isomers of neutral and anionic B_{20} clusters. They carried out highly accurate MP4(SDQ) and CCSD(T) calculations, yielding the same energy ordering for the neutral B_{20} isomers. They also show that the neutral double-ring B_{20} isomer has a large negative NICS (nucleus-independent chemical shifts) value of −40. Both calculations show that the double-ring is the lowest-energy structure and has a large negative NICS value and therefore is strongly aromatic.

Oger et al.¹¹¹ tried to explore this question further by structurally probing boron cluster cations using a combination of collision cross section measurements and DFT calculations. They applied the genetic algorithm to search for the global minimum of boron clusters. They found that boron cluster cations undergo a transition between quasi-planar and cylindrical molecular structures at B_{16}^+ . Generally, experimentally determined collision cross sections are consistent with those calculated for global minimum structures as obtained from theory. For the cations B_{17}^+ and larger, cylindrical geometries dominate the low-energy structures (for neutral clusters, the transition from two-dimensional to double-ring structures occurs for B_{20}). Clusters of type B_{2n} take the form of a double-ring, while B_{2n+1}

TABLE 4: E_b /Atom of Small Multiring Systems at the HF-SCF and B3LYP Levels of Theory Using the STO-3G Basis Set Obtained with Gaussian 03 and Gamess_UK

structure	symmetry	E_b^{SCF} (eV)	E_b^{B3LYP} (eV)
$B_{42}(2 \times 21)$	D_{21d}	5.304	6.720
$B_{42}(3 \times 14)$	D_{14h}	5.128	6.708
$B_{48}(2 \times 24)$	D_{24d}	5.306	6.740
$B_{48}(3 \times 16)$	D_{16h}	5.316	6.716
$B_{54}(2 \times 27)$	D_{27d}	5.210	6.745
$B_{54}(3 \times 18)$	D_{18h}	5.264	6.750

merely inserts the additional boron atom into one of the rings. The Jahn–Teller effect slightly distorts the B_{2n} structures away from the ideal D_{nd} symmetry. Only one of these larger clusters, particularly the B_{23}^+ cluster, prefers a curved planar geometry. In this case, the experiment finds neither a planar nor the simplest double-ring-like structure. Instead, a mixed triple- and double-ring geometry appears to be favored. Recently, the ST from 2D quasi-planar clusters into 3D double-rings was theoretically confirmed by Mukhopadhyay.¹¹ They found that this transition occurs between the B_{16} and B_{20} clusters. Hsing et al.¹¹² reduced the structural transition area to be between the B_{18} and B_{20} clusters, using high diffusion quantum Monte Carlo and DFT methods. Both theoretical calculations are in excellent agreement with the experimental results obtained by Oger et al.³⁸

The calculations of the previous section show that the triple-ring system B_{3n} is more stable than the double-ring system B_{2n} being $n > 14$. Consequently again arises the same question: at which cluster size are the triple-ring structures more stable than those of the double-rings? Therefore, in order to understand the competition between the double-ring and triple-ring systems, we have carried out a series of calculations for both systems studying the cluster sizes for $n = 42, 48$, and 54 (Figure 7). The obtained energies and the related stability are listed in Table 4 and illustrated for the B3LYP values in Figure 9. It is to perceive that the ST from the double-ring to three-ring system occurs by the B_{48} cluster at the HF-SCF level, since the corresponding E_b/atom values of the three-ring systems 5.316 eV for B_{48} and 5.264 eV for B_{54} are larger than those of the double-ring system B_{2n} . At the B3LYP level starts the ST first by the B_{54} cluster. Therefore, one can ascertain the ST occurs from the double-ring to three-ring system between the B_{52} and B_{54} clusters (Figure 9).

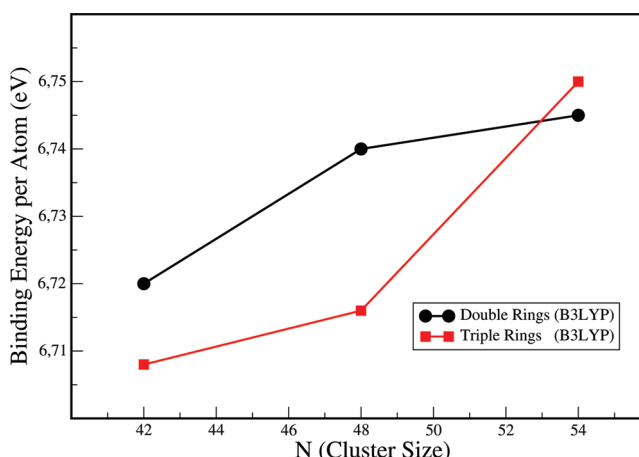


Figure 9. The structural transition from double-ring B_{2n} to triple-ring B_{3n} for $n = 42, 48$, and 54. The transition occurs at the cluster size 53.

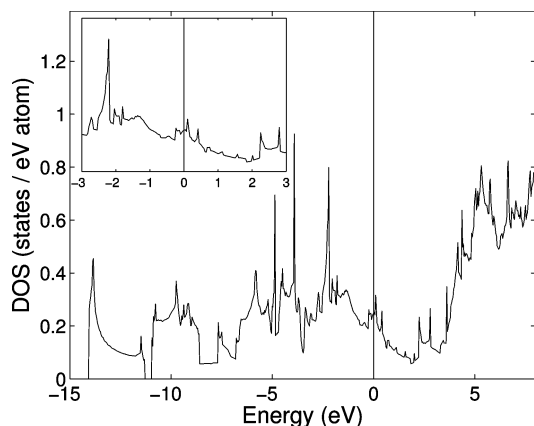


Figure 10. The density of states of the boron γ -sheet. The vertical line is the Fermi level located at the zero point energy. Inset: enlargement around the Fermi level.

7. Relative Stability and Electronic Structures. The reference energy for the stability of all calculated structures of solids and clusters is the experimental cohesive energy of solid α -rhombohedral boron, which is about 6.0 eV.⁷⁴ While the E_b/atom value 5.98 eV of the α -rhombohedral boron solid, obtained at the GGA/B3LYP and TMP (CPMD) (Table 1) is pretty close to the experimental one, raises this value to around 6.686 eV by the methods GGA/PW91 and PAW (VASP) increasing by 11.3% of the experiment value. Unfortunately, the E_b/atom value of α -boron climbs to 7.66 eV when the B3LYP/STO-3G level (Gaussian 03) is applied. Thus, it increases nearly by 28% of the experimental value. Nevertheless, all of the E_b/atom values of the clusters and strip are naturally lying below the calculated E_b/atom of α -boron (Table 3). In order to compare the relative stability of clusters to that of the strip, we depict the E_b/atom of all clusters as a function of the size (Figure 8). This diagram presents the cluster families of spheres, double-, triple-, and quadruple-ring, quasiplanar, and infinite strip of double-ring. The stability of most clusters is relatively below that of the strip except for two species: the spherical B₁₀₀ cluster and the triple-ring system. The structural transition from quasiplanar to double-ring systems is between 16 and 20, while the ST from double-ring to triple-ring systems is between 48 and 54. It is also to be recognized that the E_b/atom of the triple-ring system crosses that of the strip at $n > 70$. A general trend of the binding energies of solids and clusters calculated at different levels of theory is to be observed. A comparison of the binding energies at the HF-SCF and B3LYP(DFT) level shows that the HF-SCF values are relatively underestimated while those achieved at the B3LYP are overestimated. This confirms our comparative study of the theoretical methods HF-SCF/CI and DFT/LSD/NSD on boron clusters.¹¹³

The density of states (DOS) of the γ -, α -, and buckled-sheets are presented in Figures 10–12. These DOS show that the sheets are conductive, thus having metallic character. In contrast, the DOS of α -B₁₂ shows its semiconductor behavior, as can be seen in Figure 13. The calculated direct band gap of α -B₁₂ is 2.06 eV. It is in excellent agreement with the experimental value 2.0 eV (Table 1). The direct and indirect band gaps of α -B₁₂ boron of 2.65 and 1.50 eV, obtained at the GGA/PW91 and PAW levels (VASP) (Table 1), are over- and underestimated relative to the experimental value, respectively. The direct band gap of γ -B₂₈ of 2.08 eV, calculated at the GGA/B3LYP and TMP levels of theory (CPMD), is very close to the experimental value of 2.1 eV obtained by Zarechnaya et al.³⁰ The corresponding band structure (Figure 14) shows that the top of the

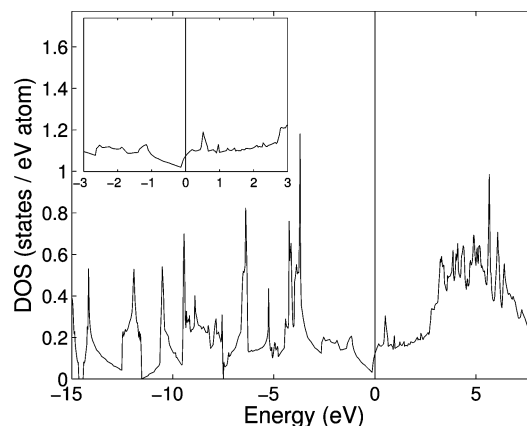


Figure 11. The density of states of the boron α -sheet. The vertical line is the Fermi level located at the zero point energy. Inset: enlargement around the Fermi level.

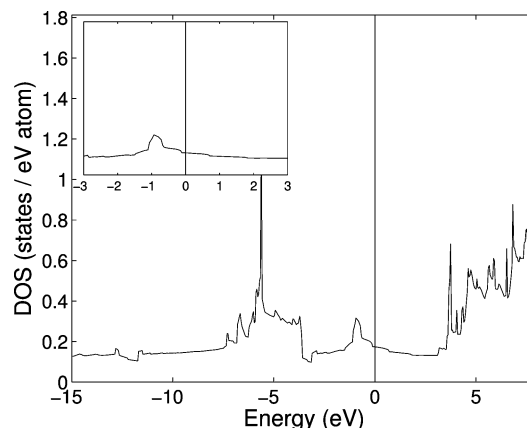


Figure 12. The density of states of the boron buckled-sheet. The vertical line is the Fermi level located at the zero point energy. Inset: enlargement around the Fermi level.

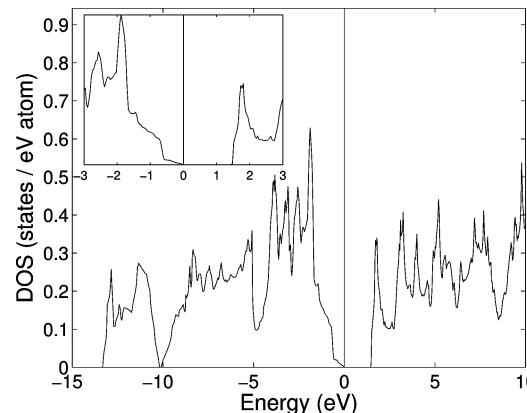


Figure 13. The density of states of the α -rhombohedral boron. The vertical line is the Fermi level located at the zero point energy. Inset: enlargement of the gap region.

valence band is at the k -point between the Γ and Z point (about 68% from Γ to Z). The energy at the Γ point is very close to -0.04 eV. The bottom of the conduction band at the T point is at the 1.87 eV energy level which is considered as the indirect band gap. The direct and indirect band gaps of γ -B₂₈, determined at the GGA/PW91 and PAW levels (VASP), are about 2.50 and 1.63 eV. The band gap values for α - and γ -boron are estimated from the DOS as 1.52 and 1.49 eV (Figures 13 and 15), respectively.

Many exciting properties of boron clusters, for instance, optical, magnetic, electron (charge) transport, and dipole po-

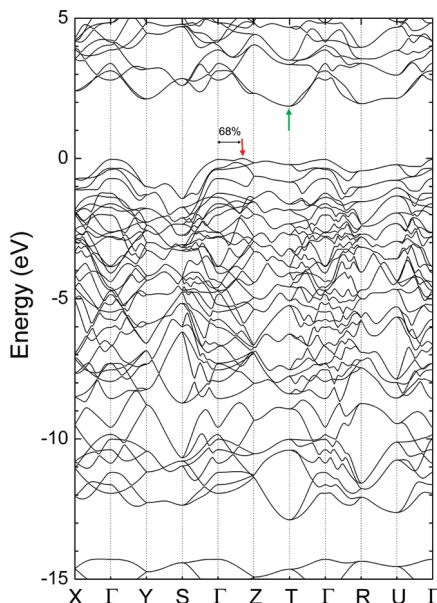


Figure 14. The band structure of γ -orthorhombic boron along the unit B_{28} . The arrows indicate the top of the valence band and the bottom of the conduction band.

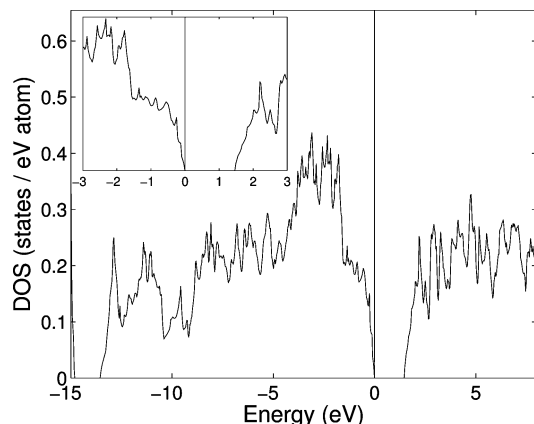


Figure 15. The density of states of γ -orthorhombic boron. The vertical line is the Fermi level located at the zero point energy. Inset: enlargement of the gap region.

larizability, are of high interest. For example, optical and magnetic properties of different boron fullerenes were studied by Botti et al.¹¹⁴ The dipole polarizability of small clusters was determined by Reis et al.¹¹⁵ and of larger boron fullerenes by Zope and Baruah.¹¹⁶ Since boron nanotubes and spheres are conductive, they were examined by their conductivity using *ab initio* methods. Hereafter, we have investigated the electron transport in boron nanotubes,¹¹⁷ in boron fullerenes B_{80} ¹¹⁸ and B_{100} ,⁹⁷ while Li¹¹⁹ in boron nanoribbons. We have shown that the electrical conductance in B_{100} is the double as in B_{80} . The wonderful idea of magnetically induced ring currents was proposed by Johansson in a B_{20} double-ring and neighboring toroids,¹²⁰ and extended to toroidal boron clusters B_{2n} for $n = 6–14$.¹²¹ Furthermore, the aromaticity, which can be obtained by NICS (method based on magnetic shielding, proposed by Schleyer et al.¹²²), is another essential property and useful quantity in evaluating the stability of boron clusters, as already verified by Zhao et al.¹²³ for B_{32} isomers. Finally, the boron α -sheets, proposed by Ismail-Beigi,⁷ seem to functionalize as a template for hydrogen storage. Brocks and co-workers¹²⁴ studied the hydrogen storage properties of planar boron sheets and compared them to those of graphene. They found that dispersion

of alkali-metal atoms like Li, Na, and K on these sheets increases the hydrogen binding energies and storage capacities.

8. Summary and Conclusions

Different morphologies of boron structures were studied using *ab initio* quantum chemical and density functional methods. Two kinds of calculations were carried out. The first kind of calculations is the noninteracting free-standing nanoclusters in the form of rings, spheres, and sheets of different sizes, and of course the elemental cells of α - B_{12} and γ - B_{28} boron. The second kind of calculations are those structures underlying periodic interacting conditions, representing infinite systems like the staggered double-rings, α - and γ -sheets, or α - B_{12} and γ - B_{28} boron solids. We have considered the measured cohesive energy of α -rhombohedral boron as a reference for all obtained energies of boron clusters and solids. The energy of the infinite strip of the double-rings was considered as the reference energy for all calculations of the free-standing clusters. Besides boron solids, we were aware to investigate nanosystems containing the same numbers of atoms so that the computations and the resulting stability are comparable. The comparison between the stability of these structures gives insight about the relationship between the solids and clusters.

Therefore, it is really amazing to develop a variety of B_{96} isomers in different forms, each belonging to a definite boron family, and compare them energetically with B_{96} of α -rhombohedral boron and B_{120} of γ -orthorhombic boron as representatives of solids. The first family is marked by the icosahedral arrangements. The first member of this family is the α -rhombohedral (α -Rh.) boron cluster (Figure 1), in which the icosahedra are located on each of the corners of the rhombohedron. The second member is the structure of icosahedra (Figure 5, upper), in which the icosahedra are distributed and connected to each other along a ring. The next family is the set of competitive 2D monolayered sheets assigned as α -sheet and γ -sheet (Figure 3), planar-sheet (not presented but calculated), and buckled-sheets (Figure 4, upper). The family of spheres, called boron fullerenes, consists of B_{80} and B_{100} (Figure 3) and of B_{96} . Both B_{100} and B_{96} cages are generated from the C_{80} fullerene (Figure 4, lower), while B_{80} was generated from the C_{60} fullerene. The multiring family, consisting of double-, triple-, quadruple-, sextuple-, and octuple-rings with different diameters, consists of 96 atoms (Figure 6). In addition, we have studied the stability of the triple-ring system B_{3n} for $n = 6, 10, 12, 18, 30$, and 40 and the quadruple-ring system B_{4n} for $n = 5, 6, 12, 18$, and 30 (Table 4). Furthermore, we have investigated the competition between the double-ring, triple-ring, quadruple-ring, quasiplanar, and spherical structures illustrated through the binding energy/atom as a function of the cluster size (Figures 8 and 9). The structural transition from a quasiplanar to double-ring structure occurs beyond 20 (Figure 8) and from a double-ring to triple-ring structure beyond 54 (Figure 9). All of these structures are deposited in the database given in ref 125.

As can be seen in Table 3, both of the icosahedral arrangements seem to be energetically unfavored. The E_b/atom values of both icosahedral arrangements in rhombohedral and ring structures at the B3LYP level are 6.366 and 6.293 eV, respectively. Thus, the ring of icosahedra has the lowest E_b/atom and consequently the lowest stability between the isomers. The α -Rh. cell is by 73 meV slightly more stable than the latter one. However, it still remains relatively unstable in relation to the reference energy of the strip, as mentioned above. The stability of the double-walled rings, composed of inner three 16-rings surrounded by two 24-rings (Figure 5), is by 331 meV

above the value of the strip. The next set of isomers are the sheets showing similar binding energies and hence similar stability to the α -Rh. cell, but the E_b/atom values of the sheets are lying below that of the strip.

In contrast, most members of the multiring system exhibit a similar stability to the strip. Only the thinnest nanotube B₉₆(8 \times 12) and the double-walled multirings B₉₆(3 \times 16 + 2 \times 24) are less stable than the strip by 371 and 331 meV, respectively. While the difference in stability of the B₉₆(6 \times 16) and B₉₆(4 \times 24) systems compared with that of the strip reduces to values of 220 and 106 meV, it decreases by the finite double-rings B₉₆(2 \times 48) to only 8 meV. The stability of both triple-rings of B₉₆(3 \times 32) and B₁₂₀(3 \times 40) exceeds slightly by only 4 and 8 meV above that of the strip. However, it is a fact that the sequence of the stability for some isomers at the HF-SCF level can be changed at the B3LYP level, where the electron exchange-correlation energy is considered. By a value of 60 meV is the structure of the double-ring B₉₆(2 \times 48) at the HF-SCF level more stable than that of the triple-ring B₉₆(3 \times 32) and even the most stable one under the tubular clusters and spheres. At the B3LYP level rises the stability of the triple-ring B₉₆(3 \times 32) only by 12 meV over the corresponding value of the double-ring B₉₆(2 \times 48) structure. This fact is also true for the stability of the double- and triple-rings of B₄₈.

In conclusion, we have studied mostly the structures, stability, and electronic properties of α -B₁₂ and γ -B₂₈ solids as well as of nanoclusters in different morphologies. The calculated cohesive energy of α -rhombohedral boron 5.98 eV, obtained at the GGA/B3LYP and TMP levels of theory and at zero temperature and pressure (CPMD), is in excellent agreement with the experimental value 6.0 eV. Hence, one can ascertain that the results of methods considered in the CPMD code for boron solids are more reliable than those considered by the VASP code. Therefore, we find that the norm-conserving Troullier–Martins-type pseudopotentials (TMP)⁷² as well as the generalized gradient approximation (GGA) by means of the functional (B3LYP) derived by Becke⁵⁷ and by Lee, Yang, and Parr,⁵⁸ used in the CPMD code provide an excellent and accurate description of the complex boron structures. In addition, the energy cutoff of 50 Ry (680 eV) for the plane-wave expansion was sufficient to provide a convergence for total energies and geometries. We find also that α -B₁₂ boron at the GGA/B3LYP and TMP (CPMD) and GGA/PW91 and PAW (VASP) levels of theory is more stable than the γ -B₂₈ boron.

The calculated indirect band gaps 2.06 and 2.08 eV of α -B₁₂ and γ -B₂₈ solids, achieved at the GGA/B3LYP and TMP levels of theory (CPMD), are very close to the experimental values 2.0 and 2.1 eV, respectively. The competition between the three boron nanosheets depends on their attitude. If the triangular buckled-sheet is considered as a free-standing noninteracting cluster, then it is more stable than both the α -sheet and γ -sheets. In contrast, if the nanosheets are considered in periodic systems, then the α -sheet is the most stable infinite system followed by the γ -sheet and buckled-sheet. However, further qualitative calculations for different sizes of boron sheets are required to verify this trend. The periodic systems of boron sheets are conductive, and the corresponding density of states (DOS) show continuous density (Figures 10–12). Independent of the number of atoms/cell, considered at the LDA and GGA levels (VASP), we confirm the results of Tang and Ismail-Beigi⁷ that the α -sheet as a periodic system is the most stable configuration of sheets.

We have generated the two spheres B₉₆ and B₁₀₀ from the C₈₀ fullerene by setting boron atoms only in 16 and 20 centers of 30 hexagons of the polyhedron C₈₀, respectively. The B₁₀₀

sphere persists at an unusual higher stability than the B₉₆ sphere of the current work and than the B₈₀ fullerene proposed by Yakobson et al.⁸ As can be seen in Figure 8 and Table 3, the spherical B₁₀₀ structure (Figure 3) remains the most stable free-standing cluster among all quasi-planar clusters, spheres, double-, triple-, and quadruple-ring systems for cluster sizes up to 120 atoms, as well as the infinite double-ring strip. Even at the B3LYP-DFT/6-31G* level,⁹⁷ the binding energy per atom of B₁₀₀ is by 10 meV higher than that of B₈₀, suggesting the former to be energetically more favored than the latter. Nevertheless, additional qualitative calculations with larger basis sets are required to verify this trend. We found that the triple-ring system B_{3n} is more stable than the infinite strip of the double-ring system when the cluster size is larger than 70. The members of the B₉₆ family give insight about the sequence or hierarchy of the stability according to Table 3 as follows: icosahedral arrangements < sheets < multirings or nanotubes \leq B₁₀₀ fullerene.

The embryonal structural transition of small boron clusters from the quasi-planars 2D into the double-ring smallest and thinnest nanotubes 3D occurs between the B₁₆ and B₂₀ clusters. Here, we determined the next structural transition from the double-ring system B_{2n} to the three-ring system B_{3n}. This transition, calculated at the B3LYP level of theory, occurs between the B₅₂ and B₅₄ clusters. The structural transition from the triple-ring boron system B_{3n} to the boron fullerene B₁₀₀ is still unclear. The stability of clusters and solids considered at the HF-SCF/STO-3G level is underestimated relative to the experimental value, while it is overestimated when the functionals B3LYP/STO-3G as well as GGA/PW91 and PAW are considered. We believe that improving the basis set and including the configuration interaction (CI) beyond the HF-SCF would confirm this trend that HF-SCF/CI and B3LYP(DFT) respectively under- and overestimate the binding energy relative to the experiment. Some properties are still missing, like the infrared and Raman spectra of the vibrational modes of clusters. Other characteristics of interest are the thermal and thermo-electric, optical and optoelectronic, and mechanical properties, as well as electron transport and electron current in larger boron nanostructures. Finally, since the potential applications of boron nanostructures like boron nanotubes, spheres, and sheets in nanotechnology is huge, characterized through their unique properties, e.g., conductivity, the experimentalists are requested and invited to challenge the synthesis and production of boron nanostructures.

Acknowledgment. We thank Dr. Jens Kunstmann for the valuable discussions and his help in reading the manuscript. Some of the computations were partly performed at Çankaya University and at the ULAKBİM High Performance Computing Center at the Turkish Scientific and Technical Research Council. I.B. acknowledges the fruitful discussions and the constructive criticism of David Tomanek as well as the support of the National Science Foundation under NSF-NSEC grant 425826.

References and Notes

- Oganov, A. R.; Chen, J.-H.; Gatti, C.; Ma, Y.-Z.; Ma, Y.-M.; Glass, C. W.; Liu, Z.-X.; Yu, T.; Kurakevych, O. O.; Solozhenko, V. L. *Nature* **2009**, 457, 863.
- Yu, E.; Dubrovinsky, L.; Dubrovinskaia, N.; Miyajima, N.; Filinchuk, Y.; Chernyshov, D.; Dmitriev, V. *Sci. Technol. Adv. Mater.* **2008**, 9, 044209.
- Boustani, I. *Phys. Rev. B* **1997**, 55, 16426.
- Boustani, I. *Surf. Sci.* **1997**, 370, 355.
- Lau, K. C.; Pandey, R. *J. Phys. Chem. C* **2007**, 111, 2906.

- (6) Boustani, I.; Quandt, A.; Hernandez, E.; Rubio, A. *J. Chem. Phys.* **1999**, *110*, 3176.
 (7) Tang, H.; Ismail-Beigi, S. *Phys. Rev. Lett.* **2007**, *99*, 115501.
 (8) Szwacki, N. G.; Sadrzadeh, A.; Yakobson, B. *Phys. Rev. Lett.* **2007**, *98*, 166804.
 (9) Sadrzadeh, A.; Pupysheva, O.; Singh, A. K.; Yakobson, B. *J. Phys. Chem. A* **2008**, *112*, 13679.
 (10) Prased, D. L. V. K.; Jemmis, E. D. *Phys. Rev. Lett.* **2008**, *100*, 165504.
 (11) Mukhopadhyay, S.; He, H.; Pandey, R.; Yap, Y. K.; Boustani, I. *J. Phys.: Conf. Ser.* **2009**, *176*, 012028.
 (12) Kunstmüller, J.; Quandt, A. *Chem. Phys. Lett.* **2005**, *402*, 21.
 (13) Zhang, Y.; Ago, H.; Yumura, M.; Ohshima, S.; Uchida, K.; Komatsu, T.; Iijima, S. *Chem. Phys. Lett.* **2004**, *385*, 177.
 (14) Tian, J.; Cai, J.; Hui, C.; Zhang, C.; Bao, L.; Gao, M.; Shen, C.; Gao, H. *Appl. Phys. Lett.* **2008**, *93*, 122105.
 (15) Wang, Z.; Shimizu, Y.; Sasaki, T.; Kawaguchi, K.; Kimura, K.; Koshizaki, N. *Chem. Phys. Lett.* **2003**, *368*, 663.
 (16) Xu, T. T.; Zheng, J.-G.; Wu, N.; Nicholls, A. W.; Roth, J. R.; Dikin, D. A.; Ruoff, R. S. *Nano Lett.* **2004**, *4*, 963.
 (17) Ding, Y.; Yang, X.; Ni, J. *Appl. Phys. Lett.* **2008**, *93*, 043107.
 (18) Boustani, I.; Quandt, A.; Kramer, P. *Europhys. Lett.* **1996**, *36*, 583.
 (19) Sabra, M. K.; Boustani, I. *Europhys. Lett.* **1998**, *42*, 611.
 (20) Fujimori, M.; Nakata, T.; Nakayama, T.; Nishibori, E.; Kimura, K.; Takata, M.; Sakata, M. *Phys. Rev. Lett.* **1999**, *82*, 4452.
 (21) Masago, A.; Shirai, K.; Katayama-Yoshida, H. *Phys. Rev. B* **2006**, *73*, 104102.
 (22) van Setten, M. J.; Uijttewaal, M. A.; de Wijs, G. A.; de Groot, R. A. *J. Am. Chem. Soc.* **2007**, *129*, 2458.
 (23) Widom, M.; Mihalkovic, M. *Phys. Rev. B* **2008**, *77*, 064113.
 (24) Ogitsu, T.; Gygi, F.; Reed, J.; Motome, Y.; Schwegler, E.; Galli, G. *J. Am. Chem. Soc.* **2009**, *131*, 1903.
 (25) Slack, G. A.; Hejna, C. I.; Garbauskas, M. F.; Kasper, J. S. *J. Solid State Chem.* **1988**, *76*, 523.
 (26) Jemmis, E. D.; Balakrishnarajan, M. M. *J. Am. Chem. Soc.* **2001**, *123*, 4324.
 (27) *Boron and Refractory Borides*; Matkovich, V. I., Ed.; Springer-Verlag: Berlin, Heidelberg, New York, 1977.
 (28) Hayami, W.; Otani, S. *J. Phys. Chem. C* **2007**, *111*, 688.
 (29) Wentorf, R. H. *Science* **1965**, *147*, 49.
 (30) Yu, E.; Dubrovinsky, L.; Dubrovinskaia, N.; Filinchuk, Y.; Chernyshov, D.; Dmitriev, V.; Miyajima, N.; El Goresy, A.; Braun, H. F.; Van Smaalen, S.; Kantor, I.; Kantor, A.; Prakapenka, V.; Hanfland, M.; Mikhaylushkin, A. S.; Abrikosov, I. A.; Simak, S. I. *Phys. Rev. Lett.* **2009**, *102*, 185501.
 (31) Boustani, I. *Int. J. Quantum Chem.* **1994**, *52*, 1081.
 (32) Boustani, I.; Quandt, A. *Europhys. Lett.* **1997**, *39*, 527.
 (33) Ricca, A.; Bauschlicher, C. W., Jr. *Chem. Phys.* **1996**, *208*, 233.
 (34) Jin, H. W.; Li, Q. S. *Phys. Chem. Chem. Phys.* **2003**, *5*, 1110.
 (35) Li, Q. S.; Jin, H. W. *J. Phys. Chem. A* **2002**, *106*, 7042.
 (36) Li, Q. S.; Jin, Q.; Luo, Q.; Tang, A. C.; Yu, J. K.; Zhang, H. X. *Int. J. Quantum Chem.* **2003**, *94*, 269.
 (37) Li, Q. S.; Gong, L.-F.; Gao, Z.-M. *Chem. Phys. Lett.* **2004**, *390*, 220.
 (38) Atış, M.; Özdogan, C.; Güvenç, Z. B. *Int. J. Quantum Chem.* **2007**, *107*, 729.
 (39) Atış, M.; Özdogan, C.; Güvenç, Z. B. *Chin. J. Chem. Phys.* **2009**, *22*, 380.
 (40) Lau, K. C.; Deshpande, M.; Pandey, R. *Int. J. Quantum Chem.* **2005**, *102*, 656.
 (41) Hu, X.; Gu, F.; S Li, Q. *Prog. Nat. Sci.* **1998**, *8*, 57.
 (42) Gu, F. L.; Yang, X.; Tang, A.-C.; Jiao, H.; Schleyer, P. v. R. *J. Comput. Chem.* **1998**, *19*, 203.
 (43) Aihara, J.-I.; Kanno, H.; Ishada, T. *J. Am. Chem. Soc.* **2005**, *127*, 13324.
 (44) Fowler, J. E.; Ugalde, J. M. *J. Phys. Chem. A* **2000**, *104*, 397.
 (45) Kiran, B.; Kumar, G. G.; Nguyen, M. T.; Kandalam, A. K.; Jena, P. *Inorg. Chem.* **2009**, *48*, 9965.
 (46) Aihara, J.-I. *J. Phys. Chem. A* **2001**, *105*, 5486.
 (47) Cao, P.-L.; Zhao, W.; Li, B.-X.; Song, B.; Zhou, X.-Y. *J. Phys.: Condens. Matter* **2001**, *13*, 5065.
 (48) Zhai, H. J.; Kiran, B.; Li, J.; Wang, L. S. *Nat. Mater.* **2003**, *2*, 827.
 (49) Zhai, H.-J.; Wang, L. S.; Alexandrova, A. N.; Boldyrev, A. I.; Zakrzewski, V. G. *J. Phys. Chem. A* **2003**, *107*, 9319.
 (50) Zhai, H.-J.; Wang, L. S.; Alexandrova, A. N.; Boldyrev, A. I. *J. Chem. Phys.* **2002**, *117*, 7917.
 (51) Alexandrova, A. N.; Boldyrev, A. I.; Zhai, H.-J.; Wang, L. S.; Steiner, E.; Fowler, P. W. *J. Phys. Chem. A* **2003**, *107*, 1359.
 (52) Alexandrova, A. N.; Boldyrev, A. I.; Zhai, H.-J.; Wang, L. S. *J. Phys. Chem. A* **2004**, *108*, 3509.
 (53) Zhai, H.-J.; Alexandrova, A. N.; Birch, K. A.; Boldyrev, A. I.; Wang, L. S. *Angew. Chem., Int. Ed. Engl.* **2003**, *42*, 6004.
 (54) Alexandrova, A. N.; Boldyrev, A. I.; Zhai, H.-J.; Wang, L. S. *Coord. Chem. Rev.* **2006**, *250*, 2811.
 (55) Hohenberg, P.; Kohn, W. *Phys. Rev. B* **1964**, *136*, 864.
 (56) Kohn, W.; Sham, L. J. *Phys. Rev. A* **1965**, *140*, 1133.
 (57) Becke, A. D. *J. Chem. Phys.* **1998**, *38*, 3089.
 (58) Lee, C.; Yang, W.; Parr, R. G. *Phys. Rev. B* **1988**, *37*, 785.
 (59) Guest, M. F.; Bush, I. J.; van Dam, H. J. J.; Sherwood, P.; Thomas, J. M. H.; van Lenthe, J. H.; Havenith, R. W. A.; Kendrick, J. *Mol. Phys.* **2005**, *103*, 719.
 (60) Frisch, M. J.; et al. *Gaussian 03*, revision B.03; Gaussian, Inc.: Wallingford, CT, 2004.
 (61) Kresse, G.; Hafner, J. *Phys. Rev. B* **1993**, *47*, 558; *48*, 13115.
 (62) Kresse, G.; Furthmüller, J. *Comput. Mater. Sci.* **1996**, *6*, 15; *Phys. Rev. B* **1996**, *54*, 11169.
 (63) Teter, M. P.; Payen, M. C.; Allan, D. C. *Phys. Rev. B* **1989**, *40*, 12255.
 (64) Perdew, J. P.; Wang, Y. *Phys. Rev. B* **1992**, *45*, 13244.
 (65) Perdew, J. P.; Chevary, J. A.; Vosko, S. H.; Jackson, K. A.; Pederson, M. R.; Singh, D. J.; Fiolhais, C. *Phys. Rev. B* **1992**, *46*, 6671.
 (66) Blöchl, P. E. *Phys. Rev. B* **1994**, *50*, 17953.
 (67) Kresse, G.; Joubert, D. *Phys. Rev. B* **1999**, *59*, 1758.
 (68) Quandt, A.; Özdogan, C.; Kunstmüller, J.; Fehske, H. *Nanotechnology* **2008**, *19*, 335707.
 (69) CPMD, <http://www.cpmd.org/>, Copyright IBM Corp 1990–2008, Copyright MPI für Festkörperforschung Stuttgart 1997–2001.
 (70) Marx, D.; Hutter, J. *NIC Series*; John von Neumann Institute for Computing: Jülich, Germany, 2000; Vol. 1, pp 301–449.
 (71) Car, R.; Parrinello, M. *Phys. Rev. Lett.* **1985**, *55*, 2471.
 (72) Troullier, N.; Martins, J. L. *Phys. Rev. B* **1991**, *43*, 1993.
 (73) Monkhorst, H. J.; Pack, J. D. *Phys. Rev. B* **1976**, *13*, 5188.
 (74) CRC, *Handbook of Chemistry and Physics*; Lide, D. R., Ed.; CRC Press: Boca Raton, FL, 1995.
 (75) Golikova, O. A.; Solovev, N. E.; Ugai, Y. A.; Feigelman, V. A. *J. Less-Common Met.* **1981**, *82*, 362.
 (76) Horn, F. H. *J. Appl. Phys.* **1959**, *30*, 1611.
 (77) Solozhenko, V. L.; Kurakevych, O. O.; Oganov, A. R. *J. Superhard Mater.* **2008**, *30*, 84.
 (78) Jiang, C.; Lin, Z.; Zhang, J.; Zhao, Y. *Appl. Phys. Lett.* **2009**, *94*, 191906.
 (79) Dubrovinskaia, N.; Dubrovinsky, L.; Yu, E.; Filinchuk, Y.; Chernyshov, D.; Dmitriev, V.; Mikhaylushkin, A. S.; Abrikosov, I. A.; Simak, S. I. arXiv:0907.1900.
 (80) Oganov, A. R.; Chen, J.-H.; Gatti, C.; Ma, Y.-Z.; Ma, Y.-M.; Glass, C. W.; Liu, Z.-X.; Yu, T.; Kurakevych, O. O.; Solozhenko, V. L. arXiv: 0908.0489.
 (81) Henkelman, G.; Arnaldsson, A.; Jónsson, H. *Comput. Mater. Sci.* **2006**, *36*, 254.
 (82) Evans, M. H.; Joannopoulos, J. D.; Pantelides, S. T. *Phys. Rev. B* **2005**, *72*, 045434.
 (83) Cabria, I.; Alonso, J. A.; Lopez, M. J. *Phys. Status Solidi A* **2006**, *203*, 1105.
 (84) Kunstmüller, J.; Quandt, A. *Phys. Rev. B* **2006**, *74*, 035413.
 (85) Boustani, I.; Quandt, A. *Comput. Mater. Sci.* **1998**, *11*, 132.
 (86) Lau, K. C.; Pandey, R. *J. Phys. Chem. C* **2007**, *111*, 2906.
 (87) Yang, X.; Ding, Y.; Ni, J. *Phys. Rev. B* **2008**, *77*, 041402(R).
 (88) Lau, K. C.; Pandey, R. *J. Phys. Chem. B* **2008**, *112*, 10217.
 (89) Boustani, I. *J. Solid State Chem.* **1997**, *133*, 182.
 (90) Yan, Q.-B.; Zheng, Q.-R.; Su, G. *Phys. Rev. B* **2008**, *77*, 224106.
 (91) Liu, A. Y.; Zope, R. R.; Pederson, M. R. *Phys. Rev. B* **2008**, *78*, 155422.
 (92) Yan, Q.-B.; Sheng, X.-L.; Zheng, Q.-R.; Zhang, L.-Z.; Su, G. *Phys. Rev. B* **2008**, *78*, 201401(R).
 (93) Szwacki, N. G. *Nanoscale Res. Lett.* **2008**, *3*, 49.
 (94) Zope, R. R.; Baruah, T.; Lau, K. C.; Liu, A. Y.; Pederson, M. R.; Dunlap, B. I. *Phys. Rev. B* **2009**, *79*, 161403(R).
 (95) Zope, R. R. *Europhys. Lett.* **2009**, *85*, 68005.
 (96) Boustani, I.; Rubio, A.; Alonso, J. A. *Chem. Phys. Lett.* **1999**, *311*, 21.
 (97) He, H.; Pandey, R.; Boustani, I.; Karna S. *J. Phys. Chem. C*, in press.
 (98) Chacko, S.; Kanhere, D. G.; Boustani, I. *Phys. Rev. B* **2003**, *68*, 035414.
 (99) Kunstmüller, J.; Quandt, A.; Boustani, I. *Nanotechnology* **2007**, *18*, 155703.
 (100) Lau, K. C.; Pati, R.; Pandey, R.; Pineda, A. C. *Chem. Phys. Lett.* **2006**, *418*, 549.
 (101) Singh, A. K.; Sadrzadeh, A.; Yakobson, B. I. *Nano Lett.* **2008**, *8*, 1314.
 (102) Sebetci, A.; Mete, E.; Boustani, I. *J. Phys. Chem. Solids* **2008**, *69*, 2004.

- (103) Lau, K. C.; Orlando, R.; Pandey, R. *J. Phys.: Condens. Matter* **2008**, *20*, 125202.
- (104) Boustani, I.; Quandt, A.; Rubio, A. *J. Solid State Chem.* **2000**, *154*, 269.
- (105) Ciuparu, D.; Klie, R. F.; Zhu, Y.; Pfefferle, L. *J. Phys. Chem. B* **2004**, *108*, 3967.
- (106) Tian, F.-Y.; Wang, Y.-X. *J. Chem. Phys.* **2008**, *129*, 024903.
- (107) Kiran, B.; Bulusu, S.; Zhai, H.-J.; Yoo, S.; Zeng, X. C.; Wang, L. S. *Proc. Natl. Acad. Sci. U.S.A.* **2005**, *102*, 961.
- (108) Marques, M. A. L.; Botti, S. *J. Chem. Phys.* **2005**, *123*, 014310.
- (109) Lau, K. C.; Pandey, R. *Comput. Lett.* **2005**, *1*, 259.
- (110) An, W.; Bulusu, S.; Gao, Y.; Zeng, X. C. *J. Chem. Phys.* **2006**, *124*, 154310.
- (111) Oger, E.; Crawford, N. R. M.; Kelting, R.; Weis, P.; Kappes, M. M.; Ahlrichs, R. *Angew. Chem., Int. Ed.* **2007**, *46*, 8503.
- (112) Hsing, C. R.; Wei, C. M.; Drummond, N. D.; Needs, R. J. *Phys. Rev. B* **2009**, *79*, 245401.
- (113) Boustani, I. *Chem. Phys. Lett.* **1995**, *233*, 273.
- (114) Botti, S.; Castro, A.; Lathiotakis, N. N.; Andrade, X.; Marques, M. A. L. *Phys. Chem. Chem. Phys.* **2009**, *11*, 4523.
- (115) Reis, H.; Papadopoulos, M. G.; Boustani, I. *Int. J. Quantum Chem.* **2000**, *78*, 131.
- (116) Zope, R. R.; Baruah, T. *Phys. Rev. B* **2009**, *80*, 033410.
- (117) Lau, K. C.; Pandey, R.; Pati, R.; Karna, S. P. *Appl. Phys. Lett.* **2006**, *88*, 212111.
- (118) He, H.; Pandey, R.; Boustani, I.; Karna, S. Proceedings of the 8th IEEE Conference on Nanotechnology, Aug 18–21, 2008; p 500.
- (119) Li, G. Q. *Appl. Phys. Lett.* **2009**, *94*, 193116.
- (120) Johansson, M. P. *J. Phys. Chem. C* **2009**, *113*, 524.
- (121) Bean, D. E.; Fowler, P. W. *J. Phys. Chem. C* **2009**, *113*, 15569.
- (122) Schleyer, P. v. R.; Maerker, C.; Dransfeld, A.; Jiao, H.; van Eikema Hommes, N. J. R. *J. Am. Chem. Soc.* **1996**, *118*, 6317.
- (123) Zhao, Y.-Y.; Zhang, M.-Y.; Chen, B.-G.; Zhang, J.; Sun, C.-C. *THEOCHEM* **2006**, *759*, 25.
- (124) Er, S.; de Wijs, G. A.; Brocks, G. *J. Phys. Chem. C* **2009**, *113*, 18962.
- (125) <http://siber.cankaya.edu.tr/boron/>.

JP911641U